ARTICLES
PUBLISHED ONLINE: 31 JULY 2011 | DOI: 10.1038/NGEO1210

nature geoscience

Rupture of deep faults in the 2008 Wenchuan earthquake and uplift of the Longmen Shan

Wang Qi[1,2★†], Qiao Xuejun[2†], Lan Qigui[3†], Jeffrey Freymueller[4★], Yang Shaomin[1,2], Xu Caijun[5★], Yang Yonglin[6], You Xinzhao[7], Tan Kai[2] and Chen Gang[1]

At the Longmen Shan, the eastern flank of the Tibetan Plateau rises 6,000 m above the Sichuan basin within a distance of just 100 km. The mechanisms responsible for building this remarkable topographic contrast are debated. Before the 2008 Wenchuan earthquake, the Longmen Shan had experienced no documented large earthquakes and exhibited minimal shortening of the crust, leading to the proposal that flow of weak rock in the lower crust may instead drive inflation of the crust. Here we use high-resolution geodetic data to explore fault geometry, as well as the pattern of strain accumulation and release associated with the Wenchuan earthquake. We find that most of the earthquake slip occurred in the shallow crust, accommodated by two steeply dipping fault planes. We suggest that the maximization of slip in shallow crustal layers was caused by the accumulation of strain energy left over from past blind earthquakes that did not rupture the surface. Furthermore, we document slip of about 2–6 m on a deep, sub-horizontal décollement fault that extends for 60 km beneath the Longmen Shan, implying that east Tibet has been thrust over the Sichuan basin. We conclude that infrequent, large earthquakes do accommodate crustal shortening across the eastern edge of the Tibetan Plateau, lending less support to the hypothesis that inflation of the lower crust uplifts the Longmen Shan.

Mountain building often involves a large-scale thrust along which a strong plate is underthrust beneath mountain ranges to accommodate crustal shortening[1]. As a consequence, the crustal thickening is confined to the hanging wall through folding and faulting with a subsurface ramp-décollement structure[2,3]. However, the Longmen Shan on the eastern edge of the Tibetan Plateau is notable for the presence of a remarkable topographic contrast despite very low present-day convergence rates and modest shortening at the surface[4–6]. The active fold-and-thrust belt in the foothills is not associated with a large-scale low-angle thrust system[6]. This has inspired a different view of the evolution of east Tibet, in which the mid-lower crust is injected by crustal material extruded outward from the interior of Tibet owing to the collision between India and Asia[4], and this inflation of the lower crust uplifts the Longmen Shan[5]. In this model, crustal-scale thrust faults accommodate only differential uplift across the range front[6], rather than being part of a thrust system with a ramp-décollement geometry[3]. Determining how these thrust faults behave during great ruptures may shed light on the mechanisms of the growth of the Tibetan Plateau. Studying the coseismic rupture is particularly important because the interseismic deformation is so slow that it provides no effective constraints on the fault geometry.

The 12 May 2008 M_w7.9 Wenchuan, China, earthquake[7] ruptured two sub-parallel reverse faults 15–20 km apart[8–10]—the Beichuan fault (BCF) and the Pengguan fault (PGF) in the Longmen Shan (Fig. 1). The earthquake exhibited a unilateral ∼340 km-long rupture striking NE–SW with thrust and right-lateral components on a high-angle fault dipping to the NW (ref. 8). Surface breaks of 240–275 km-long on the BCF and 70–80 km-long on the PGF (refs 8–10) were identified with maximum slips of 6–11 m. Previous models[11–20] inverted from either teleseismic waveforms recorded at Global Seismic Network stations, or surface displacements in the epicentral region imaged primarily by Interferometric Synthetic Aperture Radar (InSAR), captured the first-order characteristics of earthquake rupture, such as the slip maximum beneath the Beichuan and Yingxiu towns, two of the most heavily damaged regions, with tens of thousands of casualties in the 2008 event. These source models showed differences in detail owing to the diverse strategies of data selection, data weighting, fault geometry and imposed smoothing, but all of the models suffered from limited resolution owing to a lack of precise three-dimensional observations of ground deformation close to the destruction zone. Our near-field Global Positioning System (GPS) displacements complement the InSAR data, revealing new details of the slip distribution and fault geometry that further constrain aspects of the rupture process.

Slip model constrained by geodetic data

Our post-earthquake GPS campaigns, as part of quick response surveys[21], were initiated soon after the mainshock, with most of the surveys finished within 1–2 months. Additional measurements were made intermittently for almost one year. The observations involved a total of 506 geodetic markers (Fig. 1 and Supplementary Figs S1–S2). Details of our measurements and data processing are described in Methods and Supplementary Information. Based on dislocations in an elastic half-space[22], a refined slip model is inverted from these data (Supplementary Table S1), together with available spirit levelling and InSAR measurements. We adopted a cylindrical ramp-décollement structure[8,23], characterized by the

[1]Centre of Space Research, China University of Geosciences, Wuhan, 430074, China, [2]Institute of Seismology, China Earthquake Administration & Hubei Earthquake Administration, Wuhan, 430071, China, [3]First Institution of Survey Engineering, Sichuan Bureau of Surveying & Mapping, Chengdu, 610100, China, [4]Geophysical Institute, University of Alaska, Fairbanks, Alaska, 99775, USA, [5]School of Geodesy and Geomatics, Wuhan University, Wuhan, 430079, China, [6]Survey Engineering Institution, Sichuan Earthquake Administration, Ya'an, 625000, China, [7]National Infrastructure of Earthquake Centre, Beijing, 100036, China. [†]These authors contributed equally to this work. *e-mail: wangqi@cug.edu.cn; jeff.freymueller@gi.alaska.edu; cjxu@whu.edu.cn.

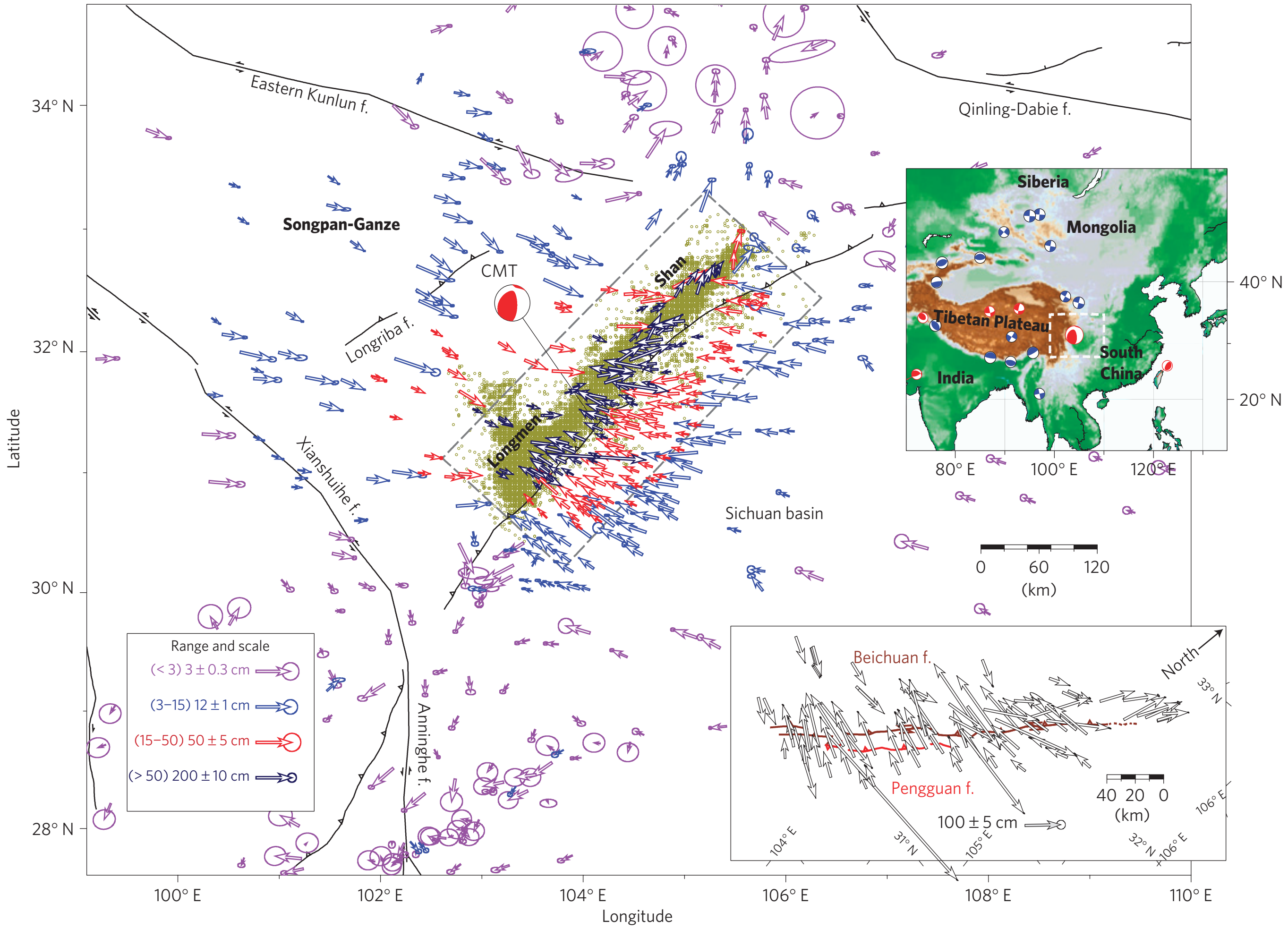

Figure 1 | Tectonic setting and surface deformation inferred from GPS measurements. Displacement vectors are depicted using differently scaled arrows with 95% confidence ellipses (2σ). The solid black lines denote major faults, and the dark yellow circles show aftershocks. The fault plane solution of the earthquake (red 'beach ball') is from the GCMT project (http://www.globalcmt.org). The lower right inset shows an up-close view of the epicentral area outlined by the dashed box. The brown and red lines mark surface rupture. The upper right inset shows regional topography as well as $M_w > 7.5$ instrumental (red) and $M \sim 8$ historic earthquakes (blue) since ~1900.

rupture plane becoming more shallowly dipping with depth and being approximated by $\sim 4 \times 4\,\mathrm{km}^2$ subfault patches to resolve the distribution of slip on it (Fig. 2). We varied the initial fault dip and fault curvature, including also faults with constant dip, and found that the best fit to the data (Fig. 2) comes from a model in which the ramp faults dip steeply near the surface and sole into a sub-horizontal décollement at depths of 15–22 km.

The best-fitting model (Supplementary Table S2 Model A) shows that the main rupture including slip >2 m corresponds to an along-strike rupture of 291–307 km from Wolong to Qingchuan (Fig. 3c), shorter than the extent of aftershocks, but significantly longer than the mapped surface rupture[8]. The geodetic inversion also requires continued slip in a region as wide as 70–80 km downdip from surface breaks along the southwest part of the BCF. Total geodetic moment released by this earthquake amounts to 9.82×10^{20} N m, assuming a rigidity of 30 GPa, equivalent to an M_w7.96 event.

With a smoothing weight $32\,\mathrm{km}^2\,\mathrm{m}^{-1}$ imposed in the inversion, our preferred model features a heterogeneous slip pattern with a total of 13 discrete asperities identified with local peak slip of >2 m (Table 1), corresponding to M_w6.5–7.4 subevents. The model shows little slip, if any, overlapping with the isoseismic areas of the historic M6–7 earthquakes[24]. Major aftershocks ($M_L > 4$) from the regional network and relocated smaller events[25] are found to cluster characteristically around the major asperities (Fig. 3a,c). In particular, the Hongkou and Caopo asperities correlate well with the aftershocks in the sense that their slip orientations are consistent with focal mechanisms of reverse or left-lateral faulting[26].

Despite the refined resolution, our model cannot recognize robustly isolated asperities or slip gaps less than 10 km in dimension. We tested a range of smoother and rougher models for comparison (Supplementary Figs S8–S10). In general, the small to medium sized asperities (for example Lixian, Maoxian, Sazhou and Chaping, Table 1) in our preferred model could be smoothed out in the highly smoothed models (for example Supplementary Table S2 Model B and Fig. S9b), whereas the large asperities remain. No single level of smoothing is ideal for all purposes. Smoother models provide more robust estimates of quantities such as maximum slip, but also suppress real heterogeneity in the slip distribution and result in significant misfits to near-fault data. Our preferred model is chosen based on a misfit-roughness tradeoff curve (Supplementary Fig. S7), such that smoother models have much higher data misfit without substantially lower model roughness; rougher models do not fit the data much better. Our preferred model reveals the spatial variation of the slip pattern, but further averaging might be applied when interpreting the slip on any individual element.

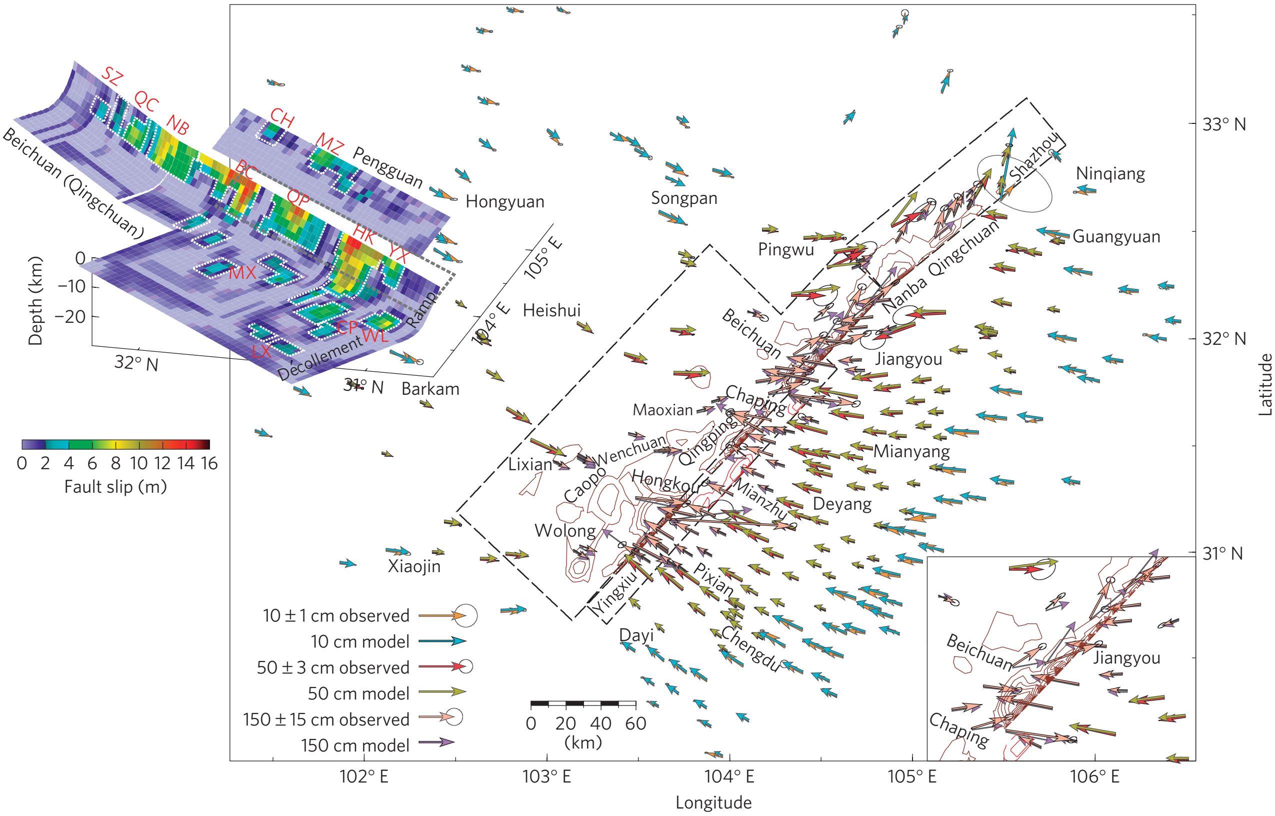

Figure 2 | Slip distribution inverted from the surface displacements. Displacement vectors are depicted using differently scaled arrows with 95% confidence ellipses (2σ). The dashed box outlines the surface projections of the faults. The contours (brown : BCF, red : PGF) denote asperities projected on the map. The upper left inset shows perspective views of outlined asperities (white dashed lines) at the viewpoint azimuth and elevation (225°, 30°). The PGF is offset deliberately eastward, with the grey dashed line representing its true position. Slip (>2 m) is illustrated by the inset colour bar. The lower right inset shows slip distribution and surface displacements around Beichuan in detail.

Comparison with the previous models

We compare our model with three representative geodetic models[14–16]. These models found 3–4 main asperities with local peak slip of 6–12 m on the BCF (similar to our Hongkou, Qingping, Beichuan, and Nanba asperities). Two of these models masked out moderate asperities (Yingxiu, Wolong and Qingchuan) at both ends of the rupture[14,16]. In all three models, slip on the BCF decreased rapidly with depth to ~20 km. Our result agrees broadly with them on the locations and slip orientations of these shallow asperities, although some important details differ. We find maximum slip of 12–13 m concentrated on very shallow parts of the BCF, similar to Tong *et al.*'s solution[16]. Shen *et al.*[14] and Feng *et al.*[15] yielded maximum slips of only 6–7 m, and the resulting regions with the peak slip are larger in dimension than those in Tong *et al.*'s model[16] and our own, indicative of stronger model smoothing.

Tong *et al.*[14] incorporated vertical components of surface offsets, which helped identify an asperity of peak slip >4 m on the PGF (Mianzhu). Like Shen *et al.*[14] and Feng *et al.*[15], we used no surface offsets to partition slip between the BCF and PGF, however the present dataset can distinguish slip between these two faults without the geologic constraints. Incorporating the mapped offsets into our modelling increased the misfit to the near-field data (Supplementary Figs S11,S19b). It is noted that the vertical components of our model are broadly compatible at the surface with the geologic offsets along most of the BCF, except at one place close to Beichuan where a vertical throw of 10–11 m was found[10]. However, geologists reported heaves that were nowhere larger than the predictions of our preferred model (Fig. 4a).

Although more highly smoothed models (128–2,048 $km^2\ m^{-1}$) reduce surface slips to some extent, discrepancies between these models and surface offsets remain in the horizontal component, even with very strong smoothing (Fig. 4a). These discrepancies are found in two areas, near Beichuan and near Nanba. Inspection of the near-fault data in these areas shows large displacements requiring significant shallow strike-slip motion, so the geodetic and geologic observations are fundamentally in conflict. It is plausible that the geologic measurements might have missed some parts of subsurface slip[10] because thrusting earthquakes usually produce abundant secondary features that absorb locally a considerable fraction of that slip[27], or it may be partitioned broadly onto parallel faults[28]. Alternatively, the strike-slip component may have decreased abruptly over a very short distance near the surface, perhaps owing to velocity-strengthening behaviour[29], a feature that our model cannot resolve.

Slip pattern and geometric irregularities on the faults

Our model reveals regions of very low slip adjacent to the asperities on the shallow part of the BCF. Such a peak-and-trough slip pattern requires spatial variations in either fault strength or pre-seismic loading, such that the stresses in the slip gaps are low enough that dynamic stresses associated with the rupture do not push them over the failure threshold[29]. The four shallow large asperities (Hongkou, Qingping, Beichuan and Nanba) correspond mostly to simple structures—continuous and straight parts of the BCF (Fig. 3a). This contrasts with the finding of Shen *et al.*[14] that the slip maxima were associated with fault junctions, which led them to suggest that the rupturing of barriers was a cause of the growth of this earthquake. Our model suggests that the fault junctions actually correspond to slip minima between the asperities. Moreover, two marked geometrical irregularities[9] are associated

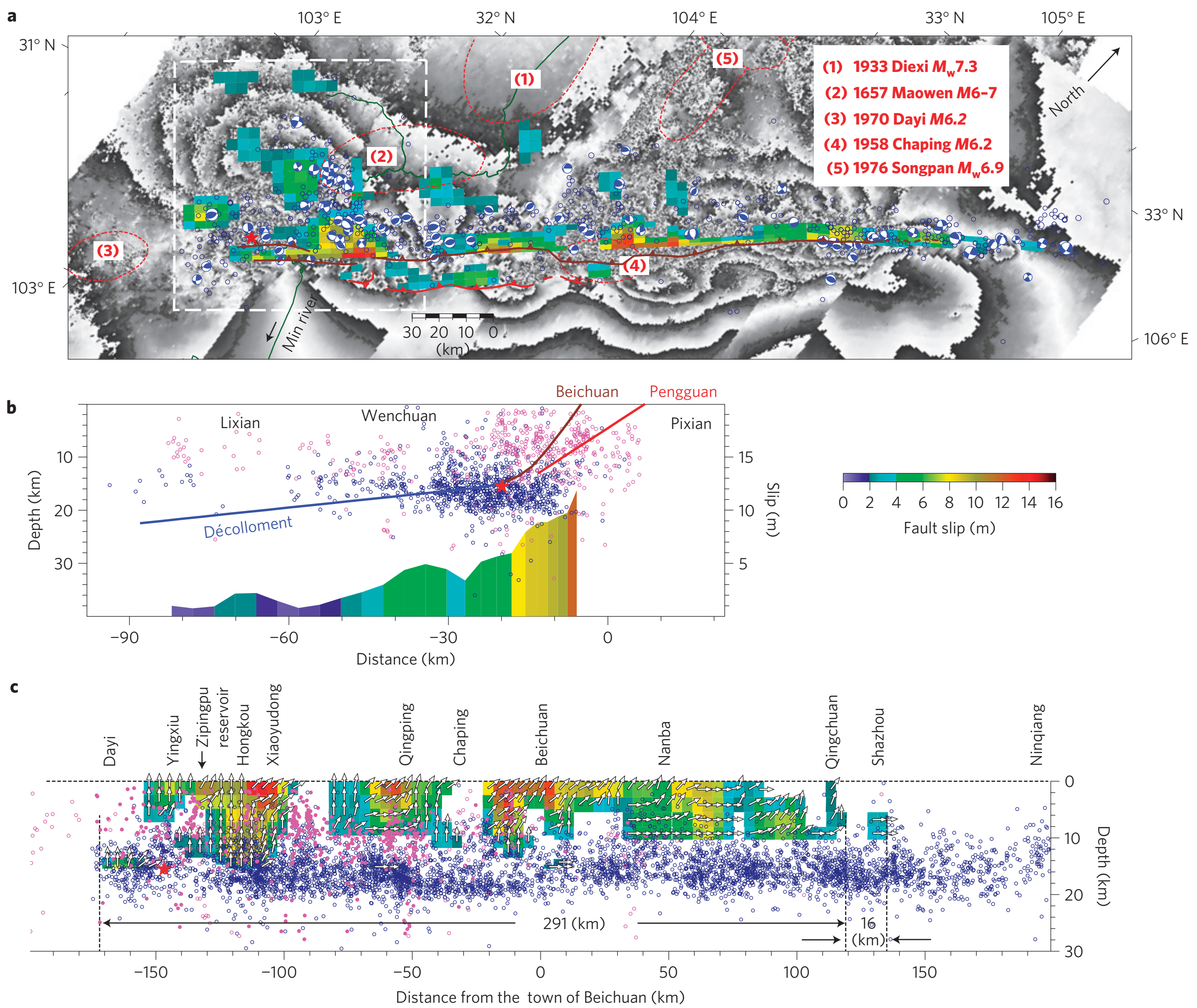

Figure 3 | Relationship between slip distribution and seismicity. a, Map-view of the slip model and InSAR fringes of LOS range changes. Aftershocks with $M_L > 4.0$ are shown. The red dashed lines delineate isoseismic areas of $M > 6$ historic earthquakes[24]. The blue 'beach balls' define focal mechanisms of $M_L > 4$ aftershocks[26]. **b**, Along-dip cross-section of fault geometry and seismicity within the dashed white box in **a**. The coloured envelope shows downdip slip from averaging 5 maximum slip patches per row of the Hongkou asperity. **c**, Along-strike cross-section of the model. The rupture length is between 291 and 307 km with white arrows indicating slip rakes. In all panels, the pink circles represent relocated earthquakes (1992–2007) with ~15 km cutoff depth[30], the blue circles show 106-day aftershocks that were confined to 5–24 km in depth[25], and the red asterisks mark hypocentres or epicentres determined by the China Earthquake Administration[12].

with low-slip gaps (<2 m) and also correlate with both endpoints of the surface break on the PGF.

At the first locality (Xiaoyudong), the BCF has a left-step offset of at least 10 km, and a tear fault branches out with up to 2–3 m of slip[8–10]. Lack of surface rupture on this fault junction (Fig. 4a) and intense $M_L > 4$ aftershocks at depths of 10–20 km suggest a strong shallow barrier that survived a complete brittle failure (Fig. 3c). The 1657 M6–7 Maowen earthquake[24] may have produced a stress shadow on neighbouring faults that contributed to impeding slip through this barrier (Fig. 3a). At the second locality (Chaping), the BCF bends clockwise 45° from its general strike[8], and bends again close to the epicentral zone of the 1958 M6.2 Chaping earthquake[24], as manifested by a remarkable trace departure (3–5 km to the southeast) from the rest of the fault[9]. Negligible background seismicity[30] and few aftershocks on this 12–16 km-long intervening segment suggest a weak barrier with low pre-seismic loading (able to accommodate stress increases induced by this mainshock without any failure, but broken in intermediate-sized earthquakes).

Matching the fault irregularities at the surface with the shallow slip gaps implies that structural complexities on the BCF may play a primary role in impeding or arresting rupture propagation[29,31,32]. Slip on the next asperity could have been dynamically triggered rather than representing passage of a single through-going rupture front. Geometrical complexities can result in variations in pre-seismic loading that have significant effects on the dynamic interaction of faults[33], but lack of knowledge of the timing of slip prevents us from assessing whether a partial stress shadow from slip on one segment might have affected the stress state on another during the earthquake itself.

Alternatively, the barriers may have failed in the sense that slip was partitioned by intensive subsidiary faulting in numerous directions[31], therefore resulting in off-fault non-brittle deformation

NATURE GEOSCIENCE DOI: 10.1038/NGEO1210

Table 1 | Characteristics of main asperities inverted from geodetic data.

Asperity	YX	HK	QP	BC	NB	QC	SZ	CP	WL	LX	MX	MZ	CH
Position (Long.)	103.41	103.62	104.06	104.47	104.87	105.40	105.40	103.36	103.21	103.16	103.82	103.98	104.36
Position (Lat.)	30.97	31.17	31.54	31.91	32.26	32.63	32.63	31.24	30.94	31.47	31.54	31.32	31.68
Moment (10^{19} Nm)	2.3	15.0	8.8	12.4	9.3	3.1	0.8	6.2	2.8	0.7	2.2	2.6	0.9
Magnitude (M_w)	6.88	7.42	7.26	7.36	7.28	6.96	6.58	7.16	6.93	6.54	6.87	6.91	6.59
Area (km^2)	16 × 12	59 × 12	44 × 12	51 × 12	48 × 12	23 × 12	10 × 12	39 × 16	20 × 16	5 × 16	21 × 16	20 × 12	7 × 12
Mean slip (m)	4.0	7.1	5.4	6.9	5.5	3.7	2.3	3.5	3.9	3.0	2.7	3.6	3.5
Peak slip (m)	6.3	12.6	11.2	12.7	9.7	5.5	2.5	6.5	6.4	3.1	3.5	5.8	4.0

SZ, Shazhou, QC, Qingchuan. NB, Nanba. BC, Beichuan. QP, Qingping. HK, Hongkou. YX, Yingxiu. MX, Maoxian. CP, Caopo. WL, Wolong. LX, Lixian. MZ, Mianzhu. CH, Chaping. The asperity area equals the area of a subfault (12 or 16 km^2) multiplied by the number of subfaults in an asperity. The peak slip corresponds to a value averaged over the three maximum slips of fault patches within an asperity.

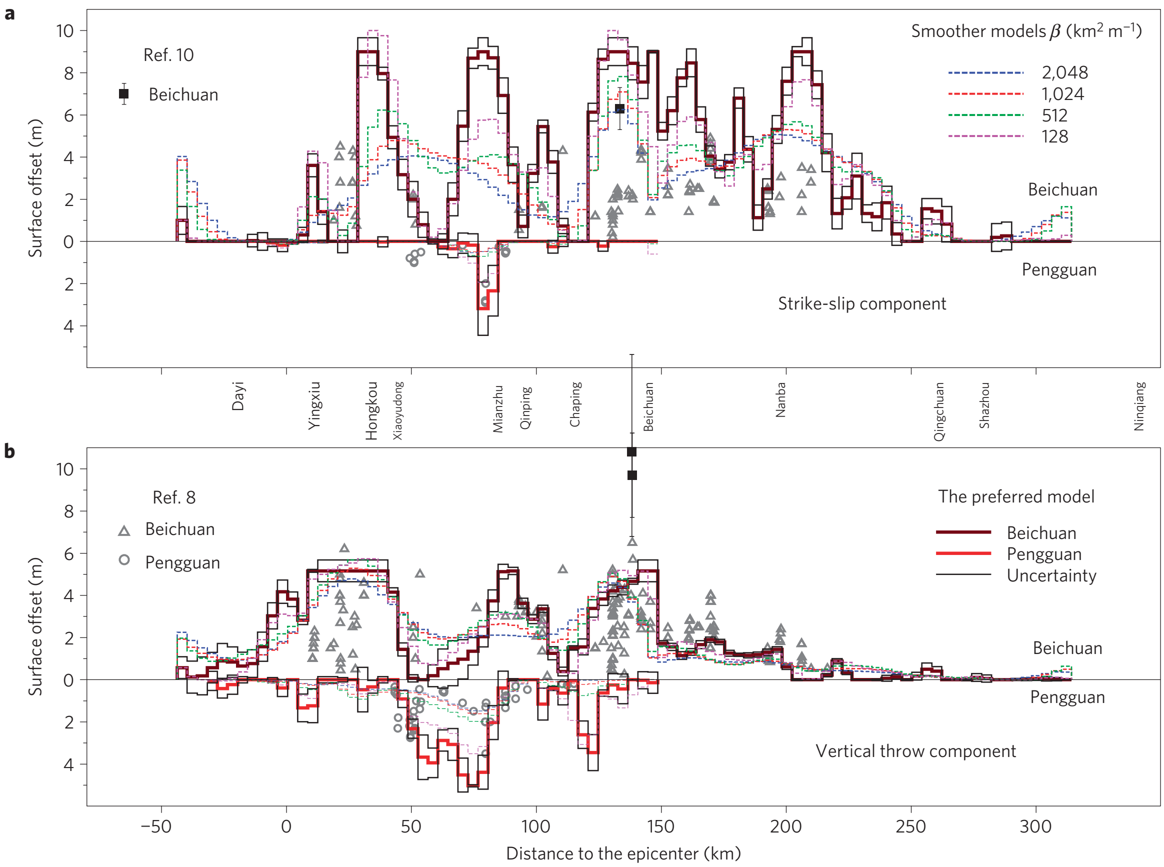

Figure 4 | Comparison between geologic surface rupture and geodetic slip models. As illustrated by the lower right inset, slip estimates (brown or solid red lines) and 2σ uncertainties (thin black lines) of the top row of the subfault matrix are used as the proxy of model surface slip to compare surface offsets mapped by Xu *et al.*[8] and the maximum slip breaks (with 2σ error bars) reported by Liu-Zeng *et al.*[10]. The 1σ uncertainty (up to 0.4 m) of the model surface slip is derived from test models generated by synthetic data using the boot-strap method (see Supplementary Information). Surface slips of highly smoothed models are defined by coloured dashed lines illustrated in the inset upper right legend. **a**, Strike-slip component. **b**, Vertical motion component.

which is difficult to recognize in the field[34,35]. It is also possible that the elastic dislocation model[22] is inadequate for interpretation of such a distributed inelastic failure—the slip gap may be no more than an artefact of geodetic slip models[36]. The present geodetic and geological data are not able to resolve this dilemma.

Shallow slip maximization and deep slip on the décollement

We do not find any evidence for a shallow slip deficit in the 2008 event, which is commonly observed in other crustal earthquakes[36]. On the contrary, most of the large asperities have their maximum slip at very shallow depth, over a wide range of model smoothing. Slip maximization so close to the surface is unusual for large thrust earthquakes and may be attributed to a dynamic frictional behaviour that amplified slip locally[37,38], or to enhanced shallow pre-seismic loading caused by previous blind thrust earthquakes such as the 1933 M_w7.3 Diexi and 1976 M_w6.9 Songpan earthquakes[39,40], which occurred in similar settings nearby[41]. Such blind events may leave residual strain energy at shallow depths to be released by a later event, rather than through diffused inelastic failures[36]. We favour the latter explanation but acknowledge that it is somewhat speculative at present given an incomplete record of palaeo-earthquakes in this region[24].

Our hypothesis that the 2008 Wenchuan earthquake was driven partially by releasing residual strain energy left over from earlier blind events is supported by a boundary element model, which predicts a synthetic coseismic slip distribution, driven by the stress accumulated within one earthquake cycle[42] for the ramp-décollement faults inferred from this event (see Supplementary Section SXIV). Assuming uniform elastic parameters, the model slip systematically underestimated the shallow coseismic slip, although it could predict the deeper slip well, given a reasonable recurrence interval. Our favoured explanation would resolve this apparent inconsistency and may help to understand the bimodal pattern of seismicity on convergent plate boundaries, although we do not think it can be confirmed using this event alone. Regardless of mechanism, the slip maximization near the surface suggests larger stress drops during the rupture, allowing the rupture to propagate more effectively across geometrical barriers in a cascading way[43]; the high stress drop would maximize near-field ground motions as well, contributing to the severe damage and triggered landslides witnessed in the 2008 catastrophic event.

One of the striking features of the slip distribution is that small to moderate sized patches with peak slip of 2–6 m are identified readily on a sub-horizontal décollement beneath the Longmen Shan. Resolution tests show that deep slip on an area in excess of $20 \times 20\,\mathrm{km}^2$ is a robust feature. Shen *et al.*[14] suggested a similar detachment fault at depth, but nowhere with slip larger than 2 m. Alternative models imposing a steeply dipping (>45° dip) downdip continuation of the BCF (Supplementary Fig. S19a) increased the root-mean-square (r.m.s.) misfit by ~100% compared to the preferred fault geometry. In cross-section (Fig. 3b), this deep-seated décollement coincides with a transition zone at 15–25 km depths known to have low P- and S-wave velocity anomalies with a high Poisson ratio[44]. In map view, the deep slip patches on the décollement coincide with a distinctive lobe of InSAR fringes and a bulge in the elongated aftershock belt at the southern end (Fig. 3a).

Slip on the décollement must be largely coseismic, although some afterslip could be included in our estimate. At a minimum, the two asperities close to the hypocentre unambiguously define coseismic slip, because afterslip of 6–7 m would be inconsistent with postseismic GPS observations[14]. Furthermore, the summed geodetic moment from slip shallower than 16 km depth, presumed to be predominately coseismic, accounts for only 78% of the GCMT estimate of 8.97×10^{20} Nm. The fault geometry and deep coseismic slip suggest crustal shortening across the eastern flank of the Tibetan Plateau as the primary mechanism of the growth of the Longmen Shan[3,8], and does not seem to support a lower crustal flow beneath east Tibet in building its margin[4,5].

In the Wenchuan earthquake, the deep coseismic slip at 15–22 km depths may lie below the seismogenic layer (Fig. 3c) if its base is assumed to be at 15 km, a typical value for continental faults[29]. If the seismogenic layer is thicker (20 km), as suggested by relocated aftershocks[25,45], the 2008 earthquake with a maximum width of about 60 km ruptured the entire seismogenic layer, and propagated sub-horizontally near its base for a considerable distance along a possible freely creeping zone characterized by velocity-strengthening friction[29]. The deep slip thus provides observational evidence for the constant stress-drop scaling of average slip with rupture length in earthquake physics[37,46,47].

Methods

GPS and SAR processing. The GPS data were processed with the Jet Propulsion Laboratory (JPL) software GIPSY-OASIS (ref. 48), using a simultaneous analysis of data from a regional network of permanent sites and campaign sites that results in a set of daily network solutions to infer coseismic displacements. We used eight tracks of images acquired by the phased-array-type L-band SAR (PALSAR) on board the Advanced Land Observing Satellite (ALOS) launched by the Japanese Aerospace Exploration Agency (JAXA). We processed the images using the JPL software ROI_PAC (ref. 49). The InSAR and GPS data are consistent in describing surface displacements, except for a narrow belt of 20–30 km in width containing the surface rupture (Supplementary Fig. S3).

Geodetic inversion. The rupture plane is approximated by a three-fault geometry with a ramp-and-décollement structure, as illustrated by structural cross-sections (Fig. 3b). In the fault model, the two ramp faults that emerge as the BCF and the PGF respectively are rooted into a deep-seated décollement beneath the Longmen Shan. We adjusted the fault geometry and solved for slip on each subfault (Supplementary Fig. S4). The rupture geometry was optimized by a grid search through a population of representatives from the model space, using the GPS data alone. In a search for the best fault geometry, we fixed the dip angle of the PGF at 35° to the west, and systematically varied the dip angle of the BCF, its downdip depth, and the dip angle of the décollement. For each model geometry tested, we estimated a variable slip model. The optimal geometry, based on the contoured RMS misfits of the various models (Supplementary Fig. S5), requires a 55° starting dip angle for the Yingxiu segment of the BCF and 70° for the Qingchuan segment. The décollement dips 7° to the west, coinciding with a spatial transition between the brittle crust and underlying ductile mid-crust where aftershocks are recognized to cease abruptly.

A total of 1,521 GPS displacement components (east, north or vertical displacements), 42 spirit levelling vertical displacements and 3,432 samples of InSAR line-of-sight (LOS) range changes (Supplementary Fig. S2) that were resampled uniformly from the eight InSAR interferograms were used in the final inversion. Using another resampling method for the InSAR data, for example a quad-tree resampling, had no effect on the results (Supplementary Fig. S6). We took into account the accurate LOS vector for each InSAR sample, which were assumed to be independent with a nominal uncertainty of 4 cm. We included correlated errors between the GPS components at each site, but ignored correlations between sites, which are generally small because individual site surveys were spread out over time. We scaled the GPS uncertainties by a factor of three. The best-fitting model, which includes thrust- and strike-slip components of a total of 2,061 subfault patches (Supplementary Table S2), is inverted using bounded least squares, with an upper limit of 10 m on the slip components, resulting in an average postfit residual of 4.4 cm (Fig. 2 and Supplementary Fig. S11).

Model test and resolution. We tested smoothing weights and upper bound values for the slip to evaluate their impact on the slip distribution (Supplementary Figs S7–S10). We also performed a series of model tests with synthetic data, either with observations perturbed by their uncertainties (Supplementary Fig. S12), or with predictions by synthetic sources (Supplementary Figs S13–S15). We tested the sensitivity of the model to the retention or rejection subsets of data obtained from InSAR, triangulation and geological measurements (Supplementary Figs S18–S19). From a total 900 runs with synthetic data, the uncertainty of slip model is estimated to better than 0.4 m, given the assumed smoothing. Based on checkerboard resolution tests, the present dataset could robustly retrieve asperities with slip >3 m for an extent of >12–16 km on the ramps and 16–20 km on the décollement. We also used the model resolution matrix to calculate the linear dimension of resolution on the rupture plane to access how slip details may be retrieved[50]. Given our preferred level of smoothing, shallow asperities >10 km in length and deep asperities >16–20 km in length are well resolved. Smaller asperities may be detected, but their slip would be spread over a larger area.

Boundary element model. The model includes a non-uniformly creeping detachment fault and two locked ramps with the geometry inferred from the inversion of surface displacements of the Wenchuan earthquake (Supplementary Fig. S20). In the interseismic period, the model is driven with an imposed secular slip on the creeping fault and uniform background strain to fit the geodetic-inferred surface displacements (Supplementary Figs S21–S22), and the accumulated strain is released at the end of a 2,500-year cycle with synthetic slip to match at greater depths the slip pattern of the Wenchuan earthquake.

Received 8 June 2010; accepted 20 June 2011; published online 31 July 2011; corrected online 2 August 2011

References

1. Molnar, P. & Lyon-Caen, H. Some simple physical aspects of the support, structure, and evolution of mountain belts. *Spec. Pap. Geol. Soc. Am.* **218,** 179–207 (1988).
2. Avouac, J-P. in *Advances in Geophysics* 46 (eds Dmowska, R. & Saltzman, B.) 1–80 (Elsevier, 2003).
3. Hubbard, J. & Shaw, J. Uplift of the Longmen Shan and Tibetan plateau, and the 2008 Wenchuan (M_w7.9) earthquake. *Nature* **458,** 191–194 (2009).
4. Royden, L. H. *et al.* Surface deformation and lower crustal flow in eastern Tibet. *Science* **276,** 788–790 (1997).
5. Clark, M. K. & Royden, L. H. Topographic ooze: Building the eastern margin of Tibet by lower crustal flow. *Geology* **28,** 703–706 (2000).
6. Burchfiel, B. C. *et al.* A geological and geophysical context for the Wenchuan earthquake of 12 May 2008, Sichuan, People's Republic of China. *GSA Today* **18,** 4–11 (2008).
7. Zhang, P., Wen, X., Shen, Z-K. & Chen, J. Oblique, High-angle, listric-reverse faulting and associated development of strain: The Wenchuan earthquake of May 12, 2008, Sichuan, China. *Annu. Rev. Earth Planet. Sci.* **38,** 353–382 (2010).
8. Xu, X. *et al.* Coseismic reverse- and oblique-slip surface faulting generated by the 2008 M_w7.9 Wenchuan earthquake, China. *Geology* **37,** 515–518 (2009).

9. Lin, A., Ren, Z., Jia, D. & Wu, X. Co-seismic thrusting rupture and slip distribution produced by the 2008 M_w7.9 Wenchuan earthquake, China. *Tectonophysics* **471,** 203–215 (2009).
10. Liu-Zeng, J. *et al.* Co-seismic ruptures of the 12 May 2008, M_s8.0 Wenchuan earthquake, Sichuan: East–west crustal shortening on oblique, parallel thrusts along the eastern edge of Tibet. *Earth Planet. Sci. Lett.* **286,** 355–370 (2009).
11. Ji, C. & Hayes, G. *Preliminary Result of the May 12, 2008 M_w7.9 Eastern Sichuan, China Earthquake* (USGS, 2008) Available via http://go.nature.com/oOKqoh.
12. Wang, W., Zhao, L., Li, J. & Yao, Z. Rupture process of the M_s8.0 Wenchuan earthquake of Sichuan China [in Chinese]. *Chin. J. Geophys.* **51,** 1403–1410 (2008).
13. Zhang, Y., Feng, W., Xu, L., Zhou, C. & Chen, Y. Spatio-temporal rupture process of the 2008 great Wenchuan earthquake. *Sci. China Ser. D* **52,** 145–154 (2009).
14. Shen, Z-K. *et al.* Slip maxima at fault junctions and rupturing of barriers during the 12 May 2008 Wenchuan earthquake. *Nature Geosci.* **2,** 718–724 (2009).
15. Feng, G., Hetland, E., Ding, X., Li, Z. & Zhang, L. Coseismic fault slip of the 2008 M_w7.9 Wenchuan earthquake estimated from InSAR and GPS measurements. *Geophys. Res. Lett.* **37,** L01302 (2010).
16. Tong, X., Sandwell, D. & Fialko, Y. Coseismic slip model of the 2008 Wenchuan earthquake derived from joint inversion of interferometric synthetic aperture radar, GPS, and field data. *J. Geophys. Res.* **115,** B04314 (2010).
17. Zhao, C., Chen, Z., Zhou, L., Li, Z. & Kang, Y. Rupture process of the 8.0 Wenchuan earthquake of Sichuan, China: The segmentation feature. *Chin. Sci. Bull.* **55,** 284–292 (2010).
18. Nakamura, T., Tsuboi, S., Kaneda, Y. & Yamanaka, Y. Rupture process of the 2008 Wenchuan, China earthquake inferred from teleseismic waveform inversion and forward modeling of broadband seismic waves. *Tectonophysics* **491,** 72–84 (2010).
19. Zhang, G., Qu, C., Song, X., Wang, C., Shan, X. & Hu, Q. Slip distribution and source parameters inverted from coseismic deformation derived by InSAR technology of Wenchuan M_w7.9 earthquake [in Chinese]. *Chin. J. Geophys.* **53,** 269–279 (2010).
20. Xu, C., Liu, Y., Wen, Y. & Wang, R. Coseismic slip distribution of the 2008 M_w7.9 Wenchuan earthquake from joint inversion of GPS and InSAR data. *Bull. Seismol. Soc. Am.* **100,** 2736–2749 (2010).
21. Working Group of the Crustal Motion Observation Network of China Project. Coseismic displacement field of the 2008 M_s8.0 Wenchuan earthquake determined by GPS [in Chinese]. *Sci. China Ser. D* **38.** 1195–1206 (2008).
22. Okada, Y. Surface deformation due to shear and tensile faults in a half-space. *Bull. Seismol. Soc. Am.* **75,** 1135–1154 (1985).
23. Li, Y. *et al.* Structural interpretation of the coseismic faults of the Wenchuan earthquake: Three-dimensional modeling of the Longmen Shan fold-and-thrust belt. *J. Geophys. Res.* **115,** B04317 (2010).
24. Wen, X., Zhang, P., Du, F. & Long, F. The background of historical and modern seismic activities of the occurrence of the 2008 M_s8.0 Wenchuan, Sichuan, earthquake [in Chinese]. *Chin. J. Geophys.* **52,** 444–454 (2009).
25. Chen, J. *et al.* Seismotectonics study by relocation of the Wenchuan M_s8.0 earthquake sequence [in Chinese]. *Chin. J. Geophys.* **52,** 390–397 (2009).
26. Wang, Q-C., Chen, Z. & Zheng, S. Spatial segmentation characteristic of focal mechanism of aftershock sequence of Wenchuan earthquake. *Chin. Sci. Bull.* **54,** 2263–2270 (2009).
27. King, G. & Vita-Finzi, C. Active folding in the Algerian earthquake of 10 October 1980. *Nature* **292,** 22–26 (1981).
28. Klinger, Y., Xu, X., Tapponnier, P., Van der Woerd, J., Lasserre, C. & King, G. High-resolution satellite imagery mapping of the surface rupture and slip distribution of the $M_w \sim 7.8$, 14 November 2001 Kokoxili earthquake, Kunlun fault, northern Tibet. China. *Bull. Seismol. Soc. Am.* **95,** 1970–1987 (2005).
29. Scholz, C. H. *The Mechanics of Earthquakes and Faulting* (Cambridge Univ. Press, 2002).
30. Zhu, A. *et al.* Relocation of small earthquakes in western Sichuan, China and its implications for active tectonics [in Chinese]. *Chin. J. Geophys.* **48,** 629–636 (2005).
31. King, G. & Nàbèlek, J. Role of fault bends in the initiation and termination of earthquake rupture. *Science* **228,** 984–987 (1985).
32. Wesnousky, S. Predicting the endpoints of earthquake ruptures. *Nature* **444,** 358–360 (2006).
33. Duan, B. & Oglesby, D. Heterogeneous fault stresses from previous earthquakes and the effect on dynamics of parallel strike-slip faults. *J. Geophys. Res.* **111,** B05309 (2006).
34. Rockwell, T. *et al.* Lateral offsets on surveyed cultural features resulting from the 1999 Izmit and Duzce earthquakes, Turkey. *Bull. Seismol. Soc. Am.* **92,** 79–94 (2002).
35. Klinger, Y., Michel, R. & King, G. Evidence for a barrier model from M_w7.8 Kokoxili (Tibet) earthquake slip-distribution. *Earth Planet. Sci. Lett.* **242,** 354–364 (2006).
36. Fialko, Y., Sandwell, D., Simons, M. & Rosen, P. Three dimensional deformation caused by the Bam, Iran, earthquake and the origin of shallow slip deficit. *Nature* **435,** 295–299 (2005).
37. Shaw, B. & Scholz, C. H. Slip-length scaling in large earthquake: Observations and theory and implications for earthquake physics. *Geophys. Res. Lett.* **28,** 2995–2998 (2001).
38. Oglesby, D. & Day, S. Fault geometry and the dynamics of the 1999 Chi–Chi (Taiwan) earthquake. *Bull. Seismol. Soc. Am.* **91,** 1099–1111 (2001).
39. Kan, R., Zhang, S., Yan, F. & Yu, L. Present tectonic stress field and its relation to the characteristics of recent tectonic activity in southwestern China [in Chinese]. *Acta Geophys. Sin.* **20,** 96–108 (1977).
40. Jones, L. M., Han, W., Hauksson, E., Zhang, Y. & Luo, Z. Focal mechanisms and aftershock implication of the Songpan earthquake of August, 1976, in Sichuan, China. *J. Geophys. Res.* **89,** 7697–7707 (1984).
41. Chen, S., Wilson, J. L., Deng, Q., Zhao, X. & Luo, Z. Active faulting and block movement associated with large earthquakes in the Min Shan and Longmen Mountains, northeastern Tibetan Plateau. *J. Geophys. Res.* **99,** 24025–24038 (1994).
42. Gomberg, J. & Ellis, M. Topography and tectonics of the central New Madrid seismic zone: Results of numerical experiments using a three-dimensional boundary-element program. *J. Geophys. Res.* **99,** 20299–20310 (1994).
43. Oglesby, D. Rupture termination and jump on parallel offset faults. *Bull. Seismol. Soc. Am.* **98,** 440–447 (2008).
44. Wang, Z., Fukao, Y. & Pei, S. Structural control of rupturing of the M_w7.9 2008 Wenchuan earthquake, China. *Earth Planet. Sci. Lett.* **279,** 131–138 (2009).
45. An, M., Feng, M. & Long, C. Deep ruptures around the hypocenter of the 12 May 2008 Wenchuan earthquake deduced from aftershocks observations. *Tectonophysics* **491,** 96–104 (2010).
46. King, G. & Wesnousky, S. Scaling of fault parameters for continental strike-slip earthquakes. *Bull. Seismol. Soc. Am.* **97,** 1833–1840 (2007).
47. Shaw, B. & Wesnousky, S. Slip-length scale in large earthquakes: The role of deep-penetrating slip below the seismogenic layer. *Bull. Seismol. Soc. Am.* **98,** 1633–1643 (2008).
48. Zumberge, J., Heflin, M., Jefferson, D., Watkins, M. & Webb, F. Precise point positioning for the efficient and robust analysis of GPS data from large networks. *J. Geophys. Res.* **102,** 5005–5017 (1997).
49. Rosen, P., Henley, S., Peltzer, G. & Simons, M. Updated repeat orbit interferometry package released. *Eos Trans. AGU* **85,** 47 (2004).
50. Funning, G. J., Parsons, B., Wright, T. J., Jackson, J. A. & Fielding, E. J. Surface displacements and source parameters of the 2003 Bam (Iran) earthquake from Envisat advanced synthetic aperture radar imagery. *J. Geophys. Res.* **110,** B09406 (2005).

Acknowledgements

Z. Nie, Z. Jia, W. Wang and B. Zhao took field observations. H. Liao, M. Wang, F. Du, A. Zhu, J. Chen, Q-C. Wang, H. Liu and C. Shi are greatly appreciated for their kind assistance. We are grateful to the UNAVCO for providing 6 GPS receivers. JAXA provided us free SAR data. This work has benefited from discussions with X. Wen, Y. Ran, X. Xu, H. Li and C. Ji. The project was supported by CEA, MOST, MOE, and NSFC (40674009, 40774014, 40874003) through grants to W.Q., Q.X. and X.C. We thank E. Hetland and Y. Klinger for their comments, which improved the manuscript. This is Institute of Seismology contribution: No. 482.

Author contributions

W.Q., Q.X., L.Q. and C.G. led GPS surveys. Y.X. coordinated the GPS surveys within the CMONOC. X.C., Y.Y. and W.Q. organized resurveys of triangulation network. Y.S. and W.Q. analysed GPS data. Q.X. and W.Q. processed SAR images. W.Q. and T.K. performed the modelling. W.Q. and J.F. analysed the slip model results and wrote the paper. W.Q. organized the project.

Additional information

The authors declare no competing financial interests. Supplementary information accompanies this paper on www.nature.com/naturegeoscience. Reprints and permissions information is available online at http://www.nature.com/reprints. Correspondence and requests for materials should be addressed to W.Q., J.F. or X.C.